Collocation on uniform grids

2009 J. Phys. A: Math. Theor. 42 115302

(http://iopscience.iop.org/1751-8121/42/11/115302)

IOP PUBLISHING JOURNAL OF PHYSICS A: MATHEMATICAL AND THEORETICAL

J. Phys. A: Math. Theor. **42** (2009) 115302 (14pp) doi:10.1088/1751-8113/42/11/115302

Collocation on uniform grids

Paolo Amore[1], **Francisco M Fernández**[2], **Ricardo A Sáenz**[1] **and Koen Salvo**[1]

[1] Facultad de Ciencias, CUICBAS, Universidad de Colima, Bernal Díaz del Castillo 340 Colima, Colima, Mexico
[2] INIFTA (UNLP, CCT La Plata-Conicet), Diag. 113 y 64 S/N, Sucursal 4, Casilla de Correo 16, 1900 La Plata, Argentina

E-mail: paolo.amore@gmail.com, fernande@quimica.unlp.edu.ar, rasaenz@ucol.mx and koen.salvo@gmail.com

Received 6 October 2008, in final form 22 January 2009
Published 23 February 2009
Online at stacks.iop.org/JPhysA/42/115302

Abstract
In this paper we derive four sets of sinc-like functions, defined on a finite interval and obeying different boundary conditions. The functions in each set are orthogonal and their nodes are uniformly distributed on the interval. We have applied each set to solve a large class of eigenvalue equations, with different boundary conditions, both on finite intervals and on the real line, showing that precise numerical results can be obtained efficiently and rapidly. A comparison with results available in the literature is also performed.

PACS numbers: 31.15.Md, 03.65.Ge

1. Introduction

In this paper, we introduce four sets of orthogonal functions, defined on a finite interval, and obeying different boundary conditions (periodic, antiperiodic, Dirichelt and von Neumann). The functions obtained here can be used to solve numerically a wide class of problems, including function interpolation, and eigenvalue equations, such as the Schrödinger equation, by means of a collocation approach.

Collocation methods provide in general an efficient tool to deal with the problems mentioned above, and the reader may find a vast literature on this subject both in physics and mathematics [1–10]. The discrete variable representation method (DVR) of [11] and the quadrature discretization method (QDM) of [12] also fall into this category.

In particular, the approach followed here is closely related to a previous work by some of us [10] which contains the derivation of a set of functions, called there little sinc functions (LSF), which is included in the sets discussed in this paper. As shown in [10], the collocation approach to the Schrödinger equation with LSF is extremely straightforward since the representation of the Hamiltonian operator has a simple analytic expression. This feature makes it possible

to implement a variational collocation approach which uses the invariance of the trace of the Hamiltonian to set an optimal collocation scale [9, 10], thus increasing the numerical precision of the results. In a recent paper, one of us has also extended this method to the relativistic Salpeter equation in [13], where the kinetic operator is nonlocal. The same functions have also been applied to the numerical solution of the Helmholtz equation on arbitrary domains in two dimensions in [14].

The main purpose of this paper is therefore to derive sets of functions obeying different boundary conditions, which can then be applied to the solution of the Schrödinger equation in much the same fashion as the original LSF. The functions discussed here are built using the four orthonormal sets of functions considered in [15], which obey periodic, Dirichlet, antiperiodic and von Neumann boundary conditions, respectively. As mentioned before, the set obeying Dirichlet boundary conditions leads to the LSF discussed in [10].

This paper is organized as follows: in section 2 we describe the general approach used to build sinc-like orthonormal systems; in section 3 we apply this approach to derive explicit expressions for the sinc-like functions corresponding to each set, explicitly showing that these functions generate uniform meshes; in section 4 we consider several examples of applications of our functions to problems on finite intervals, comparing our results with those available in the literature, and in section 5 we consider the Schrödinger equation on the real line; finally in section 6 we draw our conclusions.

2. Basic definitions

In this section, we describe the general approach which will be used to build sinc-like orthonormal systems of functions. Let $\{\psi_n(x)\}$ be an orthonormal complete system of functions in $L^2([a,b])$. Then the functions $\psi_n(x)$ satisfy the relations, in the sense of distributions,

$$\int_a^b \psi_n(x)\psi_m(x)\,\mathrm{d}x = \delta_{nm} \qquad \text{and} \qquad \sum_{n=0}^{\infty} \psi_n(x)\psi_n(y) = \delta(x-y),$$

where δ is the *Dirac delta* function [16]. A function $f \in L^2([a,b])$ can then be represented in this basis as

$$f(x) \sim \sum_{n=0}^{\infty} c_n \psi_n(x),$$

with convergence in $L^2([a,b])$, where the coefficients c_n are given by $c_n = \int_a^b f(x)\psi_n(x)\,\mathrm{d}x$.

We will now consider partial sums of this series, and set the *approximate representation of the Dirac delta function*

$$\delta_N(x,y) = \sum_{n=0}^{N} \psi_n(x)\psi_n(y). \tag{1}$$

It is easy to see that this function satisfies the convolution property

$$\begin{aligned}\int_a^b \delta_N(x,y)\delta_N(x,z)\,\mathrm{d}x &= \sum_{n=0}^{N}\sum_{m=0}^{N} \psi_n(y)\psi_m(z)\int_a^b \psi_n(x)\psi_m(x)\,\mathrm{d}x \\ &= \sum_{n=0}^{N} \psi_n(y)\psi_n(z) = \delta_N(y,z).\end{aligned} \tag{2}$$

We normalize this function by setting $\overline{\delta}_N(x, y) = \frac{\delta_N(x,y)}{\delta_N(x,x)}$. We note that often $\delta_N(x, x)$ turns out to be constant, as in some of the orthonormal sets that we consider in the following section.

Let us now select a discrete finite subset of points $\{x_k\}$ of the interval $[a, b] = [-L, L]$, and define the sampling functions

$$s_k(N, L, x) = \overline{\delta}_N(x_k, x). \tag{3}$$

If the x_k are chosen so that $\overline{\delta}_N(x_k, x_j) = 0$ if $k \neq j$, then, by (2) the functions s_k are orthogonal,

$$\int_{-L}^{L} s_k(N, L, x) s_j(N, L, x)\, \mathrm{d}x = \frac{\delta_{kj}}{\delta_N(x_k, x_k)}. \tag{4}$$

We use these functions to interpolate a function $f(x)$ defined on the interval $[-L, L]$ by

$$S_N f(x) = \sum_{k=0}^{N} f(x_k) s_k(N, L, x). \tag{5}$$

We can similarly interpolate the derivatives $s_k'(N, L, x)$ by the sums

$$Ds_k(N, L, x) = \sum_{j=0}^{N} c_{j,k} s_j(N, L, x),$$

where the coefficients are given by $c_{j,k} = s_k'(N, L, x_j)$. We thus obtain an interpolation of the derivative $f'(x)$ of f by the sum

$$DS_N f(x) = \sum_{k=0}^{N} \sum_{j=0}^{N} f(x_k) c_{j,k} s_j(N, L, x). \tag{6}$$

The interpolation (6) can be used to represent a general linear differential operator L by means of a matrix M_L, obtained from the matrix $(c_{j,k})$ acting on the points $f(x_k)$. Thus, the eigenvalues and eigenfunctions of L may be approximated by the respective eigenvalues and (interpolation of) eigenvectors of the matrix M_L.

3. Four orthonormal sets

In this section, we construct explicitly the functions $s_k(N, L, x)$ for four particular complete orthonormal systems of functions, namely those considered in [15] in the context of variational calculation. The first consists of the standard Dirichlet kernels of Fourier series, the second satisfies Dirichlet boundary conditions, the third 'antiperiodic' boundary conditions (we explain this later), while the fourth von Neumann conditions.

3.1. Periodic boundary conditions

We consider the standard orthonormal complete system functions in the interval $[-L, L]$ given by the trigonometric functions

$$\psi_0(x) = \frac{1}{\sqrt{2L}}, \qquad \psi_n(x) = \frac{1}{\sqrt{L}} \cos\left(\frac{n\pi x}{L}\right), \qquad \phi_n(x) = \frac{1}{\sqrt{L}} \sin\left(\frac{n\pi x}{L}\right), \tag{7}$$

with $n = 1, 2, \ldots$. The approximate representation of the Dirac delta function is then the normalized Dirichlet kernel [17]

$$\delta_N(x, y) = \sum_{k=0}^{N} [\psi_k(x)\psi_k(y) + \phi_k(x)\phi_k(y)] = \frac{1}{2L} \frac{\sin\left(\frac{(2N+1)\pi(x-y)}{2L}\right)}{\sin\left(\frac{\pi(x-y)}{2L}\right)}, \tag{8}$$

where the last formula is valid for $x \neq y$. One can see that $\delta_N(x,x) = \frac{2N+1}{2L}$, and thus the normalized functions are given by

$$\overline{\delta}_N(x,y) = \frac{1}{2N+1}\frac{\sin\left(\frac{(2N+1)\pi(x-y)}{2L}\right)}{\sin\left(\frac{\pi(x-y)}{2L}\right)}, \tag{9}$$

which of course satisfy $\lim_{y\to x}\overline{\delta}_N(x,y) = 1$.

Let us now consider a uniform grid with points $x_k = \frac{2Lk}{2N+1}$, with $k = -N,\ldots,N$. Clearly $\overline{\delta}_N(x_k,x_j) = \delta_{kj}$, and thus the functions

$$s_k(N,L,x) = \overline{\delta}_N(x,x_k) = \frac{1}{2N+1}\frac{\sin\left(\frac{(2N+1)\pi(x-x_k)}{2L}\right)}{\sin\left(\frac{\pi(x-x_k)}{2L}\right)} \tag{10}$$

$$= \frac{(-1)^k}{(2N+1)}\frac{\sin\left(\frac{(2N+1)\pi x}{2L}\right)}{\sin\left(\frac{\pi x}{2L}-\frac{\pi k}{2N+1}\right)} \tag{11}$$

satisfy

$$\int_{-L}^{+L} s_k(N,L,x)s_j(N,L,x)\,\mathrm{d}x = \frac{2L}{2N+1}\delta_{kj}. \tag{12}$$

We shall refer to this system as LSF_1.

3.2. Dirichlet boundary conditions

In this case we consider the orthonormal complete system of functions in the interval $[-L,L]$ given by

$$\psi_n(x) = \frac{1}{\sqrt{L}}\cos\left(\frac{(2n+1)\pi x}{2L}\right), \qquad \phi_n(x) = \frac{1}{\sqrt{L}}\sin\left(\frac{(n+1)\pi x}{L}\right), \tag{13}$$

for $n = 0,1,2,\ldots$. These functions satisfy the Dirichlet boundary conditions $\psi_n(\pm L) = \phi_n(\pm L) = 0$. We have

$$\begin{aligned}\delta_N(x,y) &= \sum_{k=0}^{N-1}[\psi_k(x)\psi_k(y) + \phi_k(x)\phi_k(y)] \\ &= \frac{1}{4L}\left[\frac{\sin\left(\frac{(4N+1)\pi(x-y)}{4L}\right)}{\sin\left(\frac{\pi(x-y)}{4L}\right)} - \frac{\cos\left(\frac{(4N+1)\pi(x+y)}{4L}\right)}{\cos\left(\frac{\pi(x+y)}{4L}\right)}\right],\end{aligned} \tag{14}$$

where the last formula is valid for $x \neq y$. We note that the function $\delta_N(x,x)$ is not constant in x. However, for $x_k = \frac{Lk}{N}$, one obtains $\delta_N(x_k,x_k) = \frac{N}{L}$, and we normalize (14) to obtain

$$s_k(N,L,x) = \frac{(-1)^k}{2N}\frac{\cos\left(\frac{\pi k}{2N}\right)\sin\left(\frac{N\pi x}{L}\right)}{\sin\left(\frac{\pi x}{2L}\right)-\sin\left(\frac{\pi k}{2N}\right)}. \tag{15}$$

This expression is equivalent to that contained in [10], with the only difference in notation, since N used there is twice N used here. We shall call this set LSF_2.

3.3. Antiperiodic boundary conditions

We now consider, on $[-L,L]$,

$$\psi_n(x) = \frac{1}{\sqrt{L}}\cos\left(\frac{2n+1}{2L}\pi x\right), \qquad \phi_n(x) = \frac{1}{\sqrt{L}}\sin\left(\frac{2n+1}{2L}\pi x\right), \tag{16}$$

with $n = 0, 1, 2, \ldots$. These functions satisfy the boundary conditions $\psi_n(\pm L) = 0$ and $\phi_n(L) = -\phi_n(-L) = (-1)^n/\sqrt{L}$. This time we have

$$\delta_N(x, y) = \sum_{k=0}^{N-1} [\psi_k(x)\psi_k(y) + \phi_k(x)\phi_k(y)] = \frac{1}{2L} \frac{\sin\left(\frac{N\pi(x-y)}{L}\right)}{\sin\left(\frac{\pi(x-y)}{2L}\right)}, \tag{17}$$

where, again, the last formula in the right is valid for $x \neq y$ and $\delta_N(x, x) = \frac{N}{L}$.

Choosing a mesh whose grid points are given by $x_k = Lk/N$ we obtain

$$s_k(N, L, x) = \frac{1}{2N} \frac{\sin\left(\frac{N\pi(x-Lk/N)}{L}\right)}{\sin\left(\frac{\pi(x-Lk/N)}{2L}\right)} = \frac{(-1)^k}{2N} \frac{\sin\left(\frac{N\pi x}{L}\right)}{\sin\left(\frac{\pi x}{2L} - \frac{\pi k}{2N}\right)} \tag{18}$$

We will call this set LSF_3.

3.4. von Neumann boundary conditions

We now consider the orthonormal complete system of functions on $[-L, L]$

$$\psi_0(x) = \frac{1}{\sqrt{2L}}, \qquad \psi_n(x) = \frac{1}{\sqrt{L}} \cos\left(\frac{n}{L}\pi x\right), \qquad n = 1, 2, \ldots, \tag{19}$$

$$\phi_n(x) = \frac{1}{\sqrt{L}} \sin\left(\frac{2n+1}{2L}\pi x\right), \qquad n = 0, 1, 2, \ldots. \tag{20}$$

These functions satisfy the von Neumann boundary conditions $\psi_n'(\pm L) = \phi_n'(\pm L) = 0$.

We have then

$$\begin{aligned} \delta_N(x, y) &= \sum_{k=0}^{N} [\psi_k(x)\psi_k(y) + \phi_k(x)\phi_k(y)] \\ &= \frac{1}{4L} \left(\frac{\sin\left(\frac{(4N+3)\pi(x-y)}{4L}\right)}{\sin\left(\frac{\pi(x-y)}{4L}\right)} - \frac{\cos\left(\frac{(4N+3)\pi(x+y)}{4L}\right)}{\cos\left(\frac{\pi(x+y)}{4L}\right)} \right), \end{aligned} \tag{21}$$

where the last formula is valid for $x \neq y$. We see again that $\delta_N(x, x)$ is not constant, but, if we take $x_k = \frac{2Lk}{2N+1}$, we have $\delta_N(x_k, x_k) = \frac{2N+1}{2L}$.

We can then normalize (21) to obtain

$$s_k(N, L, x) = \frac{(-1)^k}{2N+1} \frac{\cos\left(\frac{\pi k}{2N+1}\right) \sin\left(\frac{(2N+1)\pi x}{2L}\right)}{\sin\left(\frac{\pi x}{2L}\right) - \sin\left(\frac{\pi k}{2N+1}\right)}. \tag{22}$$

We will refer to this set as LSF_4.

Table 1 summarizes these results. We note that the sampling method in LSF_1 was already studied by Meyer in [18]. Also, LSF_2 was discussed by Baye in his paper [4], calling this set 'first sine basis'. It is not hard to see that our equation (14) is equivalent to Baye's (17), provided one makes the right change of variables.

4. Applications

In this section, we consider several applications of the sets obtained in the previous sections to the solution of different problems.

Table 1. Sampling functions and grids corresponding to the four different sets considered in section 3. Note that sets LSF_1 and LSF_4 and sets LSF_2 and LSF_3 share the same grids.

	x_k	$s_k(N, L, x)$
LSF_1	$\frac{2Lk}{2N+1}$	$\frac{(-1)^k}{(2N+1)} \frac{\sin\left(\frac{(2N+1)\pi x}{2L}\right)}{\sin\left(\frac{\pi x}{2L} - \frac{\pi k}{2N+1}\right)}$
LSF_2	$\frac{Lk}{N}$	$\frac{(-1)^k}{2N} \frac{\cos\left(\frac{\pi k}{2N}\right) \sin\left(\frac{N\pi x}{L}\right)}{\sin\left(\frac{\pi x}{2L}\right) - \sin\left(\frac{\pi k}{2N}\right)}$
LSF_3	$\frac{Lk}{N}$	$\frac{(-1)^k}{2N} \frac{\sin\left(\frac{N\pi x}{L}\right)}{\sin\left(\frac{\pi x}{2L} - \frac{\pi k}{2N}\right)}$
LSF_4	$\frac{2Lk}{2N+1}$	$\frac{(-1)^k}{2N+1} \frac{\cos\left(\frac{\pi k}{2N+1}\right) \sin\left(\frac{(2N+1)\pi x}{2L}\right)}{\sin\left(\frac{\pi x}{2L}\right) - \sin\left(\frac{\pi k}{2N+1}\right)}$

Table 2. First three eigenvalues of the Mathieu equation with $q = 1$.

N	E_0	E_1	E_2
5	1.859 106 208	4.371 185 066	9.077 920 259
10	1.859 108 073	4.371 300 983	9.078 368 847
Exact	1.859 108 073	4.371 300 983	9.078 368 847

4.1. Mathieu equation

We consider the Mathieu equation [20]

$$\frac{\mathrm{d}^2 y}{\mathrm{d}z^2} + (a - 2q\cos 2z)\, y = 0. \tag{23}$$

For $q > 0$ this equation admits periodic solutions, corresponding to particular values of a:

$$y(z) = y(2\pi + z). \tag{24}$$

These solutions are normalized to π:

$$\int_{-\pi}^{\pi} y^2(z)\, \mathrm{d}z = \pi. \tag{25}$$

We have assumed $q = 1$ and we have numerically solved the Mathieu equation using LSF_1, with $L = \pi$. We use LSF_1 as the solutions of (23) are periodic. In table 2 we display the first three eigenvalues using $N = 5$ and $N = 10$. In the last case, the first ten digits of the numerical results agree with the exact result. A similar behavior is observed for the wavefunctions: in figure 1 we have plotted the quantity $\Sigma(x) \equiv \log_{10}\left|\psi_0^{\mathrm{exact}}(x) - \psi_0^{(N)}(x)\right|$ obtained using LSF_1 with $N = 5, 10, 15$. Here $\psi_n^{\mathrm{exact}}(x)$ are the exact solutions of the Mathieu equation (see [20]). Note that since the solutions to equation (23) have definite symmetry, one can use a collocation approach with a reduced set of functions, which are obtained either by symmetrizing (even solutions) or antysymmetrizing (odd solutions) the elements of the set. In this way, the dimension of the matrices is halved and the same accuracy is reached with a limited computational effort.

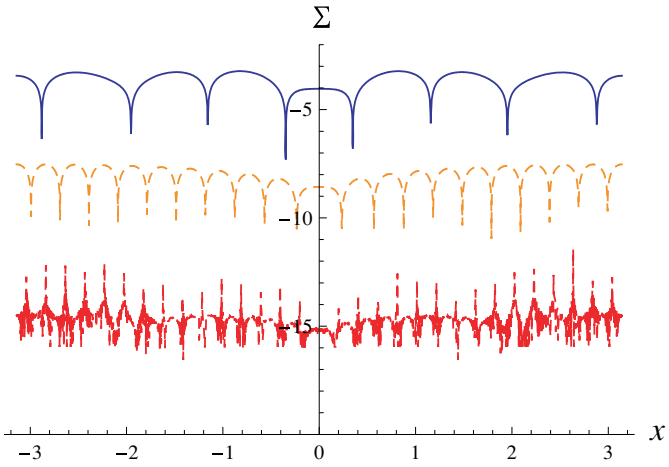

Figure 1. $\Sigma \equiv \log_{10} |\psi_0^{\text{exact}}(x) - \psi_0^{(N)}(x)|$ for the Mathieu equation obtained using LSF_1 with $N = 5, 10, 15$ (going from top to bottom).

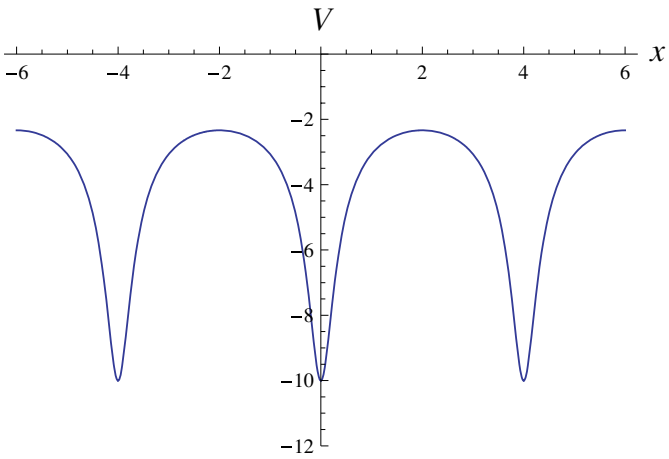

Figure 2. Periodic potential of Coulomb type of equation (26).

4.2. Truncated Coulomb-type periodic potential

Our next example is taken from [21], where the authors considered the Schrödinger equation of an electron moving in a periodic potential given by

$$V(x) = -\frac{V_0}{1+\sqrt{(a/d)^2+1}}\left[\frac{1}{\sqrt{(x/d)^2+1}} + \frac{1}{\sqrt{(x-a)^2/d^2+1}}\right], \tag{26}$$

for $0 \leqslant x \leqslant a$. Lee and Kalotas have solved the Schrödinger equation using $V_0 = 10$ eV, $a = 4$ Å, $d = 0.25$ Å. We also use $\hbar c = 197.3$ MeV fm and $m_e c^2 = 0.5$ MeV. Figure 2 shows the potential used.

In table 3, we show the numerical results for the first three eigenvalues obtained by solving the Schrödinger equation for this potential using LSF_1 and LSF_4, with $N = 40$ and $L = a$.

Table 3. Numerical solution of the Schrödinger equation for a periodic potential of Coulomb type using the LSF_1 and LSF_4 for $N = 40$.

	LSF_1	LSF_4	[21]
λ_1	−4.494 563 738	−4.494 563 738	−4.5021
λ_2	−3.204 031 703	−4.008 497 402	−3.2563
λ_3	−0.397 799 3058	−3.204 031 703	–

We have used LSF_4 as well since the potential takes its minima on integer multiples of a, and thus the solutions are expected to satisfy von Neumann conditions. The results of [21] are also reported in the last column for comparison. An important observation is that the eigenvalue λ_3 for Set I and the eigenvalue λ_2 for LSF_2 are not physically relevant: in the case of $LSF_4 \psi_2(x)$ is periodic with period $4a$, whereas in the case of LSF_1 the wavefunction $\psi_3(x)$ also obeys Dirichlet boundary conditions.

The remaining eigenvalues, calculated with the two different sets are the same to the numerical precision displayed, although obtained with different sets. We also calculated (but we prefer not to show here) the eigenvalues for this problem obtained for different grid sizes: for $N > 30$ the sequence of values is a monothonically decreasing sequence, so that we may conclude that the results reported in the table provide an upper bound to the exact results.

4.3. Unbounded periodic potential

Our next example is taken from [22], where the authors have considered the Hamiltonian

$$\hat{H} = -\frac{\mathrm{d}^2}{\mathrm{d}x^2} + \frac{\rho^2 - 1/4}{\sin^2 x} \tag{27}$$

with $\rho > 0$. The potential of this Hamiltonian is periodic with period π and singular at integer multiples of π.

The exact eigenvalues of this Hamiltonian are

$$E_n = (\rho + n + 1/2)^2 \tag{28}$$

and its exact eigenfunctions are given by

$$\psi_n(x) = \sqrt{\frac{(\rho + n + 1/2)\Gamma(2\rho + n + 1)}{n!}} \sqrt{|\sin x|} P^{-\rho}_{\rho+n}(\cos x), \tag{29}$$

where $P^{\mu}_{\nu}(x)$ are Legendre functions.

From the point of view of a numerical calculation this problem is particularly interesting because the wavefunctions in equation (29) fulfil both Dirichlet and von Neumann boundary conditions at $x = 0$ and $x = \pi$, as it can explicitly be checked. Moreover, it is easy to convince oneself, based on qualitative grounds, that the numerical solutions of the eigenvalue equation obtained using the different sets of this paper perform differently as different values of ρ are considered. In particular, for $\rho \to \frac{1}{2}^+$, the potential is small everywhere, apart from a small region around the singularities: in such case one expects that LSF_2 (Dirichlet boundary conditions) should perform better than LSF_1 or LSF_4. In the opposite regime, i.e. $\rho \gg 1$, the reverse is true, since the solutions of LSF_1 and LSF_4 have negligible values around $x = 0$ or $x = \pi$, due to the exponential suppression in the classically forbidden region, and automatically obey von Neumann boundary conditions.

In table 4 we display the numerical results obtained using the four sets both for $\rho = 0.6$ and for $\rho = 2$, with $L = \pi$. In this last case the numerical result approaches quite fastly the

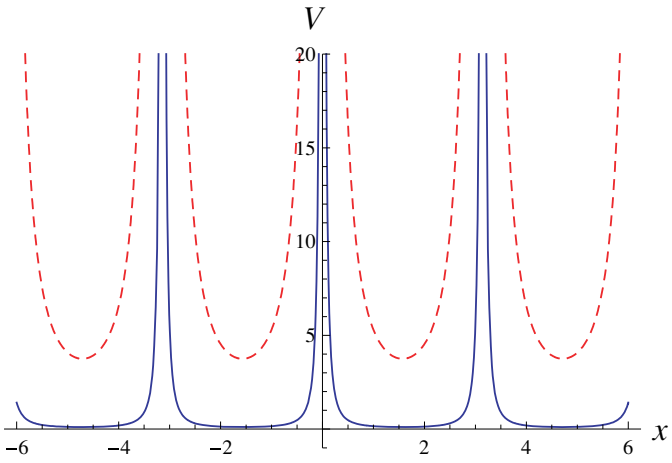

Figure 3. Periodic singular potential of [22] for $\rho = 0.6$ (solid line) and $\rho = 2$ (dashed line).

Table 4. Numerical approximation to the first eigenvalue of equation (27) for $\rho = 0.6$ (second and third columns) and $\rho = 2$ (fourth and fifth columns) using the four different sets. The row RE displays the results obtained with Richardson extrapolation of the numerical results going from $N = 10$ to $N = 40$.

N	LSF_1 and LSF_4 $\rho = 0.6$	LSF_2 and LSF_3 $\rho = 0.6$	LSF_1 and LSF_4 $\rho = 2$	LSF_2 and LSF_3 $\rho = 2$
40	1.227 120 833	1.208 720 898	6.250 001 552	6.249 999 828
80	1.217 472 028	1.209 443 039	6.250 000 099	6.249 999 989
120	1.214 598 264	1.209 657 579	6.250 000 020	6.249 999 998
RE	1.209 813 127	1.210 013 083	6.249 999 078	6.250 000 159
Exact	1.210 000 000	1.210 000 000	6.250 000 000	6.250 000 000

exact result, showed in the last row. We also display the results obtained with Richardson extrapolation of the numerical results for grids going from $N = 10$ to $N = 40$. Note that the results of columns two and three approach the exact eigenvalue from above and below respectively; similar behavior is observed for columns four and five. It is well known that basis sets with Dirichlet and von Neumann boundary conditions produce respectively upper and lower bounds to the eigenvalues [23].

4.4. Coffey–Evans equation

The Coffey–Evans equation [24–27] is a Schrödinger equation

$$-\frac{\mathrm{d}^2\psi}{\mathrm{d}x^2} + (-2\beta\cos 2x + \beta^2 \sin^2 2x)\psi(x) = \lambda\psi(x) \tag{30}$$

with $\psi(-\pi/2) = \psi(\pi/2) = 0$. Note that the example of [25] is solved on $x \in (0, \pi)$ and corresponds to $\beta = 10$. We have used this example to test the numerical accuracy of our method.

Table 5. Numerical solution of equation (30) for $\beta = 10$ using the LSF_2.

	LSF_2 $N = 20$	[25]
λ_1	0.000 000 000	0.000 000 00
λ_2	37.759 628 47	37.759 6285
λ_3	37.805 900 23	37.805 9002
λ_4	37.852 599 50	37.852 5995
λ_5	70.547 509 74	70.547 5097
λ_6	92.653 817 69	92.653 8177
λ_7	96.205 815 88	96.205 8159
λ_8	102.254 3469	102.254 347
λ_9	120.267 7566	–
λ_{10}	136.430 4340	–

Table 6. Numerical solution of the metal slab heating problem using LSF_4 with a different number of grid points.

N	λ_1	λ_2	λ_3
10	−20.000 000 00	−54.865 825 49	−84.430 478 37
20	−20.000 000 00	−54.868 669 96	−84.473 751 99
30	−20.000 000 00	−54.869 300 11	−84.477 084 62
40	−20.000 000 00	−54.869 471 60	−84.477 859 80
50	−20.000 000 00	−54.869 535 25	−84.478 132 50
60	−20.000 000 00	−54.869 563 99	−84.478 252 59
100	−20.000 000 00	−54.869 595 53	−84.478 381 85
[27]	−20	−54.8696	−84.4784

4.5. Metal slab heating problem

Our next example is taken from [27], where the eigenvalue equation

$$\frac{d^2\psi}{dx^2} - q\frac{d\psi}{dx} - g\psi(x) = \lambda\psi(x) \tag{31}$$

describing the sheet temperature profile of a metal slab. Here $x \in (0, 1)$ and $\psi'(0) = \psi'(1) = 0$. Following [27] we use the constant parameters $q = 10$ and $g = 20$. Note that the eigenfunction corresponding to the lowest eigenvalue is constant and therefore $\lambda_1 = -g$. We have collocated this problem on the uniform grid of the LSF_4, which fulfils the boundary conditions requested in this case. Table 6 contains the results for the first three eigenvalues obtained with meshes with N ranging from $N = 10$ to $N = 100$, which agree with the results obtained in [27] following a different approach.

4.6. Periodic boundary conditions

References [27, 28] contain an example of eigenvalue equation with periodic boundary conditions:

$$\frac{1}{\pi^2}\frac{d^2\psi}{dx^2} - \pi^3 x^2(1-x)\psi(x) = -\lambda\psi(x) \tag{32}$$

where $\psi(0) = \psi(1)$ and $\psi'(0) = \psi'(1)$. In table 7 we compare the eigenvalues obtained using our LSF_1, for $N = 200$, with the results of [27]. Our results agree with those of [27] to

Table 7. Numerical solution of equation (32) using the LSF of set I.

	LSF_1 $N = 200$	[27]		LSF_1 $N = 200$	[27]
λ_1	2.029 430 586	2.0294	λ_{11}	102.597 7205	–
λ_2	6.500 503 365	6.5005	λ_{12}	146.582 8816	–
λ_3	7.015 057 039	7.0151	λ_{13}	146.593 523	–
λ_4	18.584 787 01	–	λ_{14}	198.583 1142	–
λ_5	18.665 481 57	–	λ_{15}	198.590 9759	–
λ_6	38.581 643 42	–	λ_{16}	258.583 2768	–
λ_7	38.621 542 53	–	λ_{17}	258.589 3162	258.5893
λ_8	66.582 063 63	–	λ_{18}	326.583 3935	326.5834
λ_9	66.605 364 88	–	λ_{19}	326.588 1751	326.5882
λ_{10}	102.582 5421	–	λ_{20}	402.583 4797	402.5835

the accuracy reported in that paper. To be fair the numerical results of [27] are computed with only $M = 50$ discretization points, compared to our $2N + 1 = 401$ discretization points: for a given number of grid points, the method of Adomaitis and Lin however involve a series of steps which in our method are not present. As a matter of fact we are working with a uniform grid, which is specified only by the length of the interval and by the number of points and with analytical expressions for the matrices of the derivatives.

5. The Schrödinger equation on the real line

The little sinc functions discussed in this paper are defined in a finite interval $[-L, L]$ but can also be applied to eigenvalue problems on the real line $-\infty < x < +\infty$. To this end L should be sufficiently large so that a bound state is vanishingly small in the neighborhood of the end points of that region. Obviously, one has to increase both N and L in order to reach a satisfactory accuracy. From a practical point of view it is convenient to have a suitable criterion for choosing the optimum L for a given grid, i.e. with N fixed. Following [10] we propose to link the values of those parameters by means of the minimum of the trace of the Hamiltonian matrix $\mathbf{H}$: $\partial tr\mathbf{H}/\partial L = 0$. In this way, we have to increase only N and $L = L_{\mathrm{PMS}}^{(N)}$ is completely determined by the minimum condition.

As a first test of this approach we can consider the simple harmonic oscillator, for which the exact solutions are available. The implementation of the variational procedure is straightforward: working with one of the sets obtained in the previous section, we define a mesh corresponding to a given value of N. On this grid we obtain a representation of the Hamiltonian operator as a matrix whose elements are given by

$$H_{ij} = -\frac{\hbar^2}{2m} c_{ij}^{(2)} + \delta_{ij} V(x_i),$$

where x_i are the points on the grid and $c^{(2)}$ is the matrix of the second derivative. It is important to stress that the expression for H_{ij} is *analytical* and a function of L. Therefore, the trace of H is itself analytical and is obtained by summing all the diagonal elements over all the grid points. We call L_{PMS} the optimal value of L obtained by minimization of the trace. In table 8, we display the results obtained for the ground state of the simple harmonic oscillator using the four sets and grids corresponding to $N = 10, 20, 30$. The present approach provides extremely precise numerical results with all the sets considered, the first one being slightly more accurate.

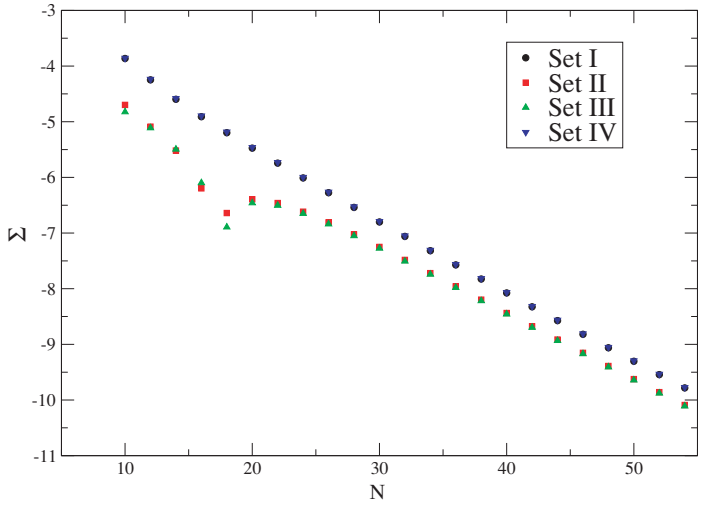

Figure 4. Logarithm of the error over the energy of the ground state of (34) $\Sigma \equiv \log_{10}|E_{\rm set}(N) - \overline{E}(100)|$ for the different sets for $\lambda = 1$. $\overline{E}(100)$ is the average of the energy of the ground state obtained with the four sets using $N = 100$.

Table 8. Variational calculation of the ground-state energy of the simple harmonic oscillator using the four different sets for $N = 10, 20, 30$.

	LSF_1	LSF_2	LSF_3	LSF_4
$L^{(10)}_{\rm PMS}$	5.743	5.718	5.751	5.643
$\Delta E_0\vert^{(10)}_{\rm PMS}$	-6.369×10^{-14}	-4.655×10^{-13}	-6.79×10^{-13}	-1.082×10^{-13}
$L^{(20)}_{\rm PMS}$	8.025	8.004	8.028	7.952
$\Delta E_0\vert^{(20)}_{\rm PMS}$	-1.981×10^{-27}	-1.423×10^{-26}	-2.148×10^{-26}	-3.439×10^{-27}
$L^{(30)}_{\rm PMS}$	9.789	9.77	9.79	9.729
$\Delta E_0\vert^{(30)}_{\rm PMS}$	-5.451×10^{-41}	-3.894×10^{-40}	-5.95×10^{-40}	-9.538×10^{-41}

The second example is the Schrödinger equation with the supersingular potential

$$H = p^2 + x^2 + \lambda\, \mathrm{e}^{x^4} \tag{34}$$

studied by Detwiler and Klauder [19]. The name of this potential comes from the fact that there is no conventional perturbation series in λ. The implementation of our method is unaffected by this feature and the approach is the same followed for the simple harmonic oscillator. In figure 4, we have displayed the logarithm of the error over the energy of the ground state of (34) $\Sigma \equiv \log_{10}|E_{\rm set}(N) - \overline{E}(100)|$ for the different sets for $\lambda = 1$. $\overline{E}(100)$ is the average of the energy of the ground state obtained with the four sets using $N = 100$. Table 9 shows the ground-state energy of the Hamiltonian operator (34) for a wide range of values of λ that span the most interesting small-λ regime. One can appreciate the advantage of the collocation methods that avoid the calculation of complicated matrix elements of the potential energy function.

Table 9. Ground-state energy of the supersingular potential of equation (34) for $\lambda = 10^q$ using the first two sets with $N = 100$.

q	$E_0^{(I)}$	$E_0^{(II)}$	$E_0^{(I)} - E_0^{(II)}$
0	2.672 270 347 028 729 4063	2.672 270 347 028 728 8917	5.15×10^{-16}
−1	1.420 268 090 317 635 9415	1.420 268 090 317 397 3972	2.39×10^{-13}
−2	1.196 097 905 799 530 4661	1.196 097 905 788 114 2875	1.14×10^{-11}
−3	1.124 587 113 656 827 7440	1.124 587 113 501 410 8365	1.55×10^{-10}
−4	1.088 423 394 773 035 8280	1.088 423 393 774 555 0839	9.99×10^{-10}
−5	1.065 879 560 082 512 3053	1.065 879 556 119 722 9543	3.96×10^{-9}
−6	1.050 519 103 881 029 9772	1.050 519 092 535 068 4659	1.13×10^{-8}
−7	1.039 537 998 985 142 9035	1.039 537 973 201 184 089	2.58×10^{-8}
−8	1.031 432 769 914 740 5618	1.031 432 720 436 772 1415	4.95×10^{-8}
−9	1.025 306 756 864 356 2956	1.025 306 673 276 254 5855	8.36×10^{-8}
−10	1.020 589 649 512 314 2124	1.020 589 521 526 953 8785	1.28×10^{-7}

6. Conclusions

In this paper we have obtained four sets of sinc-like functions, defined on finite intervals, which obey different boundary conditions. We have shown that a collocation approach to the solution of the Schrödinger equation based on these functions is both straightforward and precise and we have compared our results with those available in the literature, both for problems on the real line and for problems defined on finite intervals. In the first case we show that the collocation scheme can be used within a variational approach where the optimal scale is determined minimizing the trace of the Hamiltonian matrix, in much the same spirit of [9, 10]. We also remark that the meshes generated by the functions discussed in this paper are uniform, a desirable feature in a certain class of problems. Further applications of the sets discussed here, which will be analyzed elsewhere, include the representation of nonlocal operators on uniform meshes with different boundary conditions, and the study of the vibrations of two-dimensional membranes, as a natural extension of the work carried out in [13, 14]. Note that in this last case, the conformal mapping of the border can be handled straightforwardly within the method of [14] and yields results which rapidly converge as shown in [14].

References

[1] Schwartz C 1985 High-accuracy approximation technique for analytic functions *J. Math. Phys.* **26** 411–5
[2] Baye D and Heenen P H 1986 Generalised meshes for quantum mechanical problems *J. Phys. A: Math. Gen.* **19** 2041–59
[3] Stenger F 1993 *Numerical Methods Based on Sinc and Analytic Functions* (New York: Springer)
[4] Baye D 1995 Constant-step Lagrange meshes for central potentials *J. Phys. B: At. Mol. Opt. Phys.* **28** 4399–412
[5] Koures V G and Harris F E 1996 *Int. J. Quantum Chem.* **30** 1311
[6] Wei G W 2000 Solving quantum eigenvalue problems by discrete singular convolution *J. Phys. B: At. Mol. Opt. Phys.* **33** 343–52
[7] Easther R, Guralnik G and Hahn S 2000 *Phys. Rev.* D **61** 125001
[8] Revelli R and Ridolfi L 2003 *Comput. Math. Appl.* **46** 1443–53
[9] Amore P 2006 A variational sinc collocation method for strong coupling problems *J. Phys. A: Math. Gen.* **39** L349–55
[10] Amore P, Cervantes M and Fernández F M 2007 Variational collocation on finite intervals *J. Phys. A: Math. Theor.* **40** 13047–62
[11] Light J C, Hamilton I P and Lill J V 1985 *J. Chem. Phys.* **82** 1400–9

[12] Shizgal B D and Chen H 1996 Quadrature discretization method (QDM) in the solution of the Schrödinger equation with nonclassical basis functions *J. Chem. Phys.* **104** 4137–50
[13] Amore P 2007 Alternative representation for nonlocal operators and path integrals *Phys. Rev.* A **75** 032111
[14] Amore P 2008 Solving the Helmholtz equation for membranes of arbitrary shape: numerical results *J. Phys. A: Math. Theor.* **41** 265206
[15] Pathak R K, Chandra A K and Bhattacharyya K 1993 Functional representation in non-Fourier basis with applications *Phys. Rev.* A **48** 4097–101
[16] Griffel D H 1985 *Applied Functional Analysis* (New York: Dover)
[17] Folland G B 1999 *Real Analysis: Modern Techniques and Their Applications* (New York: Wiley)
[18] Meyer R 1970 Trigonometric interpolation method for one-dimensional quantum mechanical problems *J. Chem. Phys.* **52** 2053–9
[19] Detwiler L C and Klauder J R 1975 Supersingular quantum perturbations *Phys. Rev.* D **11** 1436–41
[20] Abramowitz M and Stegun I A 1964 *Handbook of Mathematical Functions* (New York: Dover)
[21] Lee A R and Kalotas T M 1991 Solution of the one-dimensional Schrödinger equation in an arbitrary periodic potential *Phys. Scr.* **44** 313–20
[22] Bojowald M and Swiderski R 2004 The volume operator in spherically symmetric quantum geometry *Class. Quantum Grav.* **21** 4881–900
[23] Mesón A M, Fernandez F M and Castro E A 1983 Dirichlet and von Neumann basis set for quantum mechanical anharmonic oscillators *Z. Naturforsch.* A **38** 473
[24] Coffey W T, Evans M W and Price J D 1979 The effect of dipole–dipole interaction on zero-tHz frequency polarisation *Chem. Phys. Lett.* **63** 133–8
[25] Celik I 2005 Approximate computation of eigenvalues with Chebyshev collocation method *Appl. Math. Comput.* **168** 125–34
[26] Ledoux V, Van Daele M and Vanden Berghe G 2008 Efficient computation of high index Sturm–Liouville eigenvalues for problems in physics arXiv:0804.2605
[27] Adomaitis R A and Lin Y-H 2000 A collocation quadrature based Sturm–Liouville problem solver *Appl. Math. Comput.* **110** 205–23
[28] Vanden Berghe G, Van Daele M and De Meyer H 1995 A modified difference scheme for periodic and semiperiodic Sturm–Liouville problems *Appl. Math. Comput.* **18** 69–78